Propagation of ripples in Monte Carlo models of sputter-induced surface morphology

Emmanuel O. Yewande,* Alexander K. Hartmann, and Reiner Kree
Institut für Theoretische Physik, Universität Göttingen, Friedrich-Hund Platz 1, 37077 Göttingen, Germany
(Received 17 May 2004; revised manuscript received 18 January 2005; published 9 May 2005)

Periodic ripples generated from the off-normal-incidence ion-beam bombardment of solid surfaces have been observed to propagate with a dispersion in the velocity. We investigate this ripple behavior by means of a Monte Carlo model of the erosion process, in conjuction with one of two different surface-diffusion mechanisms, representative of two different classes of materials; one is a Arrhenius-type Monte Carlo method including a term (possibly zero) that accounts for the Schwoebel effect, while the other is a thermodynamic mechanism without the Schwoebel effect. We find that the behavior of the ripple velocity and wavelength depends on the sputtering time scale, which is qualitatively consistent with experiments. Futhermore, we observe a strong temperature dependance of the ripple velocity, calling for experiments at different temperatures. Also, we observe that the ripple velocity vanishes ahead of the periodic ripple pattern.

DOI: 10.1103/PhysRevB.71.195405 PACS number(s): 68.35.−p, 05.10.−a, 79.20.−m

I. INTRODUCTION

There has been much scientific activity for quite some time now on the features of surface morphology resulting from the bombardment of a solid surface by a collimated beam of intermediate energy ions, at normal and oblique incidences to the solid surface.[1,2] The phenomenon is an essential constituent of several surface analysis, processing, and fabrication techniques, such as ion-beam-aided deposition, surface catalysis, sputter cleaning, etching, and deposition.

Normal-incidence ion bombardment of nonmetallic substrates often results in an interlocking grid of hillocks and depressions, which has been demonstrated to be an attractive alternative to the spontaneous growth of self-organized quantum dots on semiconductor surfaces in the Stranski-Krastanov growth mode.[3] Off-normal-incidence ion bombardment of such nonmetallic substrates, however, gives rise to the formation of quasiperiodic ripples[4–11] with orientations that depend on the angle of incidence of the ion beam. For incidence angles less than a critical angle θ_c (Ref. 12) the wave vectors of the ripples are parallel to the projection of the ion-beam direction on the surface plane, while for incidence angles greater than θ_c, the wave vectors of the ripples are oriented perpendicular to the projection of the ion-beam direction on the surface plane. On the other hand, ripples are observed on metallic substrates at normal-incidence ion bombardment, and these ripples are rotated by changing the substrate temperature,[13–15] a probable consequence of the symmetry-breaking anisotropy in surface diffusion. The wavelengths of the observed ripples, in all cases, is of the order of tenths of micrometers.

However, a number of experimental studies[16–19] have demonstrated that under certain ion-bombardment conditions, ripples are not formed; the surface undergoes kinetic roughening with interesting scaling properties. All these observations point to the possibility of several phases in the surface-topography evolution, with the phase boundaries defined by the bombardment conditions, and with little or no dependence on the material composition, surface chemistry, defects, or chemical reactions on the surface. These features are understood, from insightful theoretical descriptions,[2,20,21] as being governed by the interplay and competition between the dynamics of surface roughening on the one hand and material transport during surface migration on the other. Ion bombardment tends to roughen the surface, while surface diffusion leads, in general, to surface relaxation.[4,5] For sufficiently low ion energies, the sputtering phenomenon is the dominating mechanism.[2] However, if the flux is low at such energies, then the enhanced defect mobility can result in domination by surface diffusion, which may cause the overall scaling behavior of the surface profile to be uniquely determined by the nonequilibrium-biased diffusion current, independently of the microscopic origin.[22]

Recently surface ripples generated during the gallium-ion-beam erosion of silicon were observed to propagate with a ripple velocity that scaled with the ripple wavelength as $v \sim \lambda^k$, where $k \simeq 0$ initially, and $k=-1.5$ after a crossover wavelength $\lambda_c \simeq 100$ nm.[23] This velocity dispersion has been ascribed to an indication of a continuous transition to a rising nonlinear contribution in surface erosion.[2,23] Motivated by this experimental result, we study ripple propagation by means of a recently introduced, discrete, $(2+1)$-dimensional Monte Carlo (MC) model[24] of the sputtering process, and two different solid-on-solid models of surface diffusion; for details see below. We focus on intermediate times, when the transition from linear to nonlinear regimes occurs. Our results corroborate the experimental observation, but in addition we find that, at high temperatures, the ripples first come to rest before they are completely wiped out by the increasing nonlinear contributions.

The rest of the paper is organized as follows. First, we state our simulation model, i.e., how the sputtering process and the different diffusion mechanisms are implemented. Then we explain how we study the movement of the ripples. In the main section, we show our simulation results. We finish with our conclusions and an outlook.

II. EROSION AND SURFACE MIGRATION

According to Sigmund's sputtering theory,[25] the rate at which material is removed from a solid surface, through the impact of energetic particles, is proportional to the power

deposited there by the random slowing down of particles. The average energy $E(\mathbf{r}')$ deposited at surface point $\mathbf{r}'=(x',y',-z')$ is given by the Gaussian distribution,

$$E(\mathbf{r}') = \frac{\epsilon}{(2\pi)^{3/2}\sigma\mu^2}\exp\left[-\frac{(z'+d)^2}{2\sigma^2}-\frac{x'^2+y'^2}{2\mu^2}\right], \quad (1)$$

where we use the local Cartesian-coordinate system of the ion with the origin at the point of penetration, and with the z axis coinciding with the ion-beam direction. $(z'+d)$ is the distance of the surface point from final stopping point of ion measured along the ion trajectory, $\sqrt{x'^2+y'^2}$ is the distance perpendicular to it, σ and μ are the widths of the distribution parallel and perpendicular to the ion trajectory, respectively, ϵ is the total energy deposited, and d is the average depth of the energy deposition. Sigmund's formula is the basis for *all* theoretical treatments and analysis of experimental results so far.

A. The sputtering process

In the following,[24] we simulate the sputtering process on a surface of size L^2 with periodic boundary conditions by starting an ion at a random position in a plane parallel to the plane of the initially flat surface and projecting it along a straight trajectory inclined at angle θ to the normal of the average surface configuration, and at an azimuthal angle ϕ. The ion penetrates the solid through a depth d and releases its energy, such that an atom at a position $\mathbf{r}=(x,y,h)$ is eroded (see Fig. 1 of Ref. 24) with a probability proportional to $E(\mathbf{r})$. It should be noted that, consistent with the assumptions of the theoretical models,[2,20,21] this sputtering model assumes no evaporation, and no redeposition of eroded material, and no preferential sputtering of surface material at the point of penetration; the surface is defined by a single valued, discrete, time-dependent height function $h(x,y,t)$ [solid-on-solid (SOS) model]. The time t is measured in terms of the ion fluence, i.e., the number of incident ions per two-dimensional lattice site (x,y). We use incidence angle $\theta=50°$, azimuthal angle $\phi=22.0°$, $d=6.0$, $\sigma=3.0$, and $\mu=1.5$, as obtained by SRIM[26] for 5 keV Xe^+ ions on graphite, rescaling all lengths by a factor of 2. This should give, according to the linear theory of Bradley and Harper, a value of $\theta_c=68°$.[12] We have chosen ϵ to be $(2\pi)^{3/2}\sigma\mu^2$, which leads to high-sputtering yields $Y\simeq 7.0$, compared to experiments such as that in Ref. 11, where $Y=0.3,\ldots,0.5$, i.e., increasing the efficiency of the simulation. According to the Bradley-Harper theory, the ripple wavelength λ scales as $\lambda\sim Y^{-1/2}$, so that we expect patterns with correspondingly smaller length scales in our simulations. This we have to remember when quantitatively interpreting the result. Anyway, the general phenomena observed in the simulation are not affected by this choice.

Our model of the sputtering mechanism sets the time scale of the simulation and allows comparison with experiments. Additionally, also the moves of atoms mimicking surface diffusion are performed, which will be described now.

B. The Hamiltonian and Arrhenius models of surface diffusion

Surface migration is modeled as a thermally activated nearest-neighbor hopping process, as in Refs. 27 and 28. A Monte Carlo acceptance and/or rejection procedure is used for this purpose. One diffusion step refers to a complete sweep of the lattice. Two different solid-on-solid models of surface diffusion in molecular-beam epitaxy are use, the second one of them sensitive to the repulsion of a diffusing particle from a down step, and preferential diffusion in the uphill direction, which is the so-called Schwoebel effect.

The first model[27] is based on a thermodynamic interpretation of the diffusion process. For each step, a site i and one neighbor site j are randomly selected. The trial move is an atom hopping from i to j, i.e., $h_i=h_i-1$ and $h_j=h_j+1$. We calculate the surface energy before and after the hop, through the energy of an unrestricted SOS model,

$$E = \frac{J}{2}\sum_{\langle i,j\rangle}|h_i-h_j|^2. \quad (2)$$

J is a coupling constant through which the nearest-neighbor sites interact. h_i is the height variable at site i, and the summation is over the nearest neighbors on the two-dimensional substrate.

The hop is allowed with the probability,

$$p_{i\to f} = 1/\left[1+\exp\left(\frac{\Delta E_{i\to f}}{k_BT}\right)\right], \quad (3)$$

where $\Delta E_{i\to f}$ is the energy difference between the initial and final states of the move, T is the substrate temperature, and k_B is the Boltzmann's constant. Although no exact mapping is possible, we can estimate that a temperature, $k_bT/J\simeq 0.2$ in this model, corresponds roughly to the temperature used in the second model below. The estimate is based on a comparison of the pure-diffusion mechanism without sputtering such that it leads to comparable values of roughness. Note that this temperature is below the roughening transition of this model.[27] This model does not prevent atoms from moving down over step edges; hence no Schwoebel effect is present.

The second model is also based on a MC procedure and uses a formula known from kinetic MC mechanisms. For each step, again a site i and a nearest-neighbor site j are chosen at random, but now a hopping move is performed with a probability proportional to the hopping rate of an Arrhenius form,

$$k(E,T) = k_0\exp\left(-\frac{E}{k_BT}\right). \quad (4)$$

$E=E_{SB}+nnE_{NN}+E_S$ is an energy barrier to hopping, consisting of a Schwoebel barrier term E_{SB}, a substrate term $E_S=0.75$ eV and a nearest-neighbor bonding of magnitude $nnE_{NN}=nn0.18$ eV; where nn is the number of in-plane nearest neighbors of the diffusing atom. E_{SB} is equal to some constant (0.15 eV in this case. Note that we also perform runs for $E_{SB}=0$ to compare with the thermodynamic model; see below), if the numbers of next-nearest neighbors in the plane beneath the hopping atom, before (nnn_b) and after

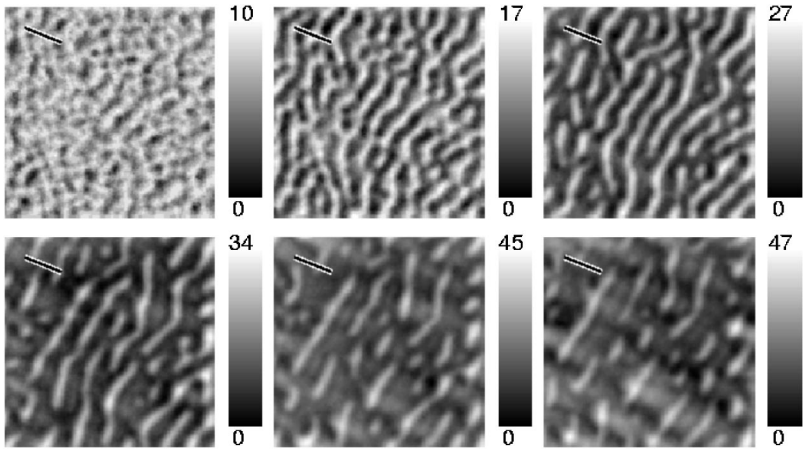

FIG. 1. Surface profiles at a substrate temperature of 0.2 J k_B^{-1} and at different times. Starting from top to bottom and left to right, $t=0.5$, 1.5, 4.0, 9.0, 14.0, and 20.0 ions/atom. The ion-beam direction, indicated by the bar, is perpendicular to the ripple orientation. The scales show the surface height measured from the lowest height.

(nnn_a) the hop, obey $4=nnn_b>nnn_a$ and zero otherwise. Our temperature is measured in units of eV k_B^{-1} in this model, where $T\simeq 0.02$ eV k_B^{-1} corresponds to room temperature. $k_0=2\ k_BT/h$ is the vibrational frequency of a surface adatom, i.e., a hopping-attempt rate, h being Planck's constant. The hopping-attempt rate is very high, with a corresponding low hopping probability resulting from Eq. (4), slowing down the simulation. Thus we incorporate the factor $\exp(-E_S/k_BT)$ into the rescaled attempt rate such that the hopping rate reads

$$k(E,T)=k_1\exp\left(-\frac{\Delta E}{k_BT}\right), \tag{5}$$

where $k_1=k_0\exp(-E_S/k_BT)$ is a much lower hopping-attempt rate, $\Delta E=nnE_{NN}+E_{SB}$. This physical attempt rate, in comparison with the ion current density used in experiments, determines the ratio between the number of sputtering steps and the number of surface-diffusion steps made in the simulation. In Sec. III, we state the values we used for our simulations. A discussion of parameter optimization and a rescaling of the temperature with the parameters is given in Ref. 29. Note finally that for atoms on top of planes that are far from down edges, i.e., $\Delta E=0$, each hop is accepted, independently of the temperature.

III. RIPPLE KINEMATICS

In experiments we typically have $N=1\times10^{15}$ atoms/cm^2 on the surface. Since the typical experimental ion current density is of the order of $F=7.5\times10^{14}$ ions/cm^2 s,[23] this implies a flux of $\Phi=F/N\simeq0.75$ ion/atom s. From the values given above, we get hopping-attempt rates k_1 of around 200×1/s for room temperature, hence 200 sweeps of the diffusion mechanism correspond to 0.75 ions per surface atom. Thus, we initiate a diffusion step every $\Phi L^2/k_1=0.0037L^2$ erosion steps; L is the system size.

Initially, for times less than about 1.4 ions/lattice site, the surface is rough[24] and then the formation of ripples starts. In this paper we focus on the motion and time development of these ripples. In Fig. 1 the time development of a sample surface topology is shown for the first diffusion model. Initially ripples are formed. They propagate slowly and, due to the increasing influence of nonlinear effects (note the scales at the right), disappear at longer times. The long-time behavior, where the ripples have disappeared, has already been studied in Ref. 24.

In order to monitor the ripple propagation on the computer, we assign the crest points of the ripples to clusters, and then monitor the motion of these clusters. A cluster of crest points is defined as the set of surface points with height $h(x,y,t)\geqslant h_c$ and nearest-neighbor distance $l\leqslant l_c$, where h_c and l_c are the cutoff surface height and distance between the neighboring cluster points, respectively. We have chosen our cutoff height to be a function of the average height of the configuration $\langle h\rangle$, and the height difference h_d between the maxima and minima of the surface; i.e, $h_c=\langle h\rangle+ph_d$, where p is a fixed percentage. In this way clusters with about the same proportionate sizes can be followed from the beginning of ripple formation until the complete disappearance of the ripples. Furthermore, we have used $l_c=2$. Different, unconnected ripples should, in general, generate different clusters. We also require that the number N of elements in a cluster be large enough to allow for statistical analysis; here we have chosen $N\geqslant10$ elements.

The propagation of the ripples is studied by calculating the time rate of change of the position of the center of mass of a cluster,

$$\dot{\mathbf{x}}_{CM}=\frac{\sum_i m_i\dot{\mathbf{x}}_i}{\sum_i m_i}, \tag{6}$$

where the summation is over all the elements of the cluster. We have assumed a homogeneous system composed of unit-mass particles, such that the center of mass of a cluster is $\mathbf{x}_{CM}=N^{-1}\Sigma_i\mathbf{x}_i$. The ripple wavelength is given by $\lambda=2\pi/\eta$, with η being the average expectation value of the Gaussian fitted to the peak of the structure factor $S(\mathbf{k})=|h(\mathbf{k})|^2$, where $h(\mathbf{k})$ is the Fourier transform of the height topography $h(\mathbf{r},t)$, given by

$$h(\mathbf{k})=\frac{1}{L^{d'/2}}\sum_{\mathbf{r}}[h(\mathbf{r},t)-\langle h\rangle]e^{i\mathbf{k}\mathbf{r}}. \tag{7}$$

d' is the substrate dimension, i.e., here $d'=2$. Figure 2 shows two profiles of the surface for system size 128×128 at time

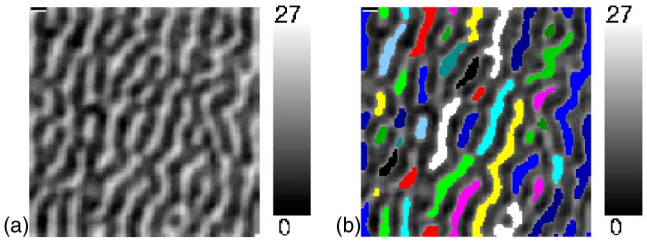

FIG. 2. (Color online) Surface profile for time 3 ions/atom (thermodynamic-diffusion model, $T=0.2\ \mathrm{J}/k_B$, $L=128$). The second profile contains the clusters formed from the first profile, as described in the text.

$t=3$ ions/atom; in the second profile, we print the clusters on top of their corresponding ripples. As seen in the figure of the clusters, the application of periodic boundary conditions neccessitates the need to first unfold the toroidal clusters before calculating the position of their centers of mass. As time increases, the local surface slopes ∇h increase, and since the nonlinear effects depend on the square of ∇h they will dominate by scaling down the surface-relaxation mechanisms.[1] These nonlinear effects are responsible for the disapearance of ripples (Fig. 1) at long times and for the transition of the surface topography from a periodic ripple pattern to a rough topography with self-affined scaling.[2,16] We thus expect fluctuations in the positions of the centers of mass due to disappearing ripples; the fluctuations are averaged out by using systems of size 512×512, with a large number of clusters such that the ripple velocity at any time is an average of the velocities of all the ripples at the time.

IV. RESULTS AND DISCUSSION

The results are obtained, as already mentioned, for square lattices of size 512×512, with periodic boundary conditions and as an average of fifty different realizations.

For the case of the Arrhenius diffusion mechanism, (including the Schwoebel barriers) one can choose a temperature corresponding to the physical temperature present in the experimental system. A naive guess is to use room temperature $k_BT=0.02$ eV, at which the experiments usually are carried through. The resulting structures are shown in Fig. 3, for intermediate as well as after long sputtering times. We cannot observe clean ripples. The reason is that this kind of diffusion mechanism is too slow at room temperature to effectively counteract the strong roughening due to our model of sputtering, which possesses a particularly high-sputtering yield. The hops are almost always prevented if an atom has in-plane neighbors, so the mechanism is not very effective on a rough surface. Since surface relaxation is essential for the formation of ripples,[20] it needs *locally* higher temperatures than room temperatures to produce clean ripples in our model. This happens indeed in experiments, since most of the kinetic energy, carried by the incoming ion, is converted into lattice vibrations; hence the surface is locally strongly heated. Here, we do not know the spatiotemporal distribution of the local temperature. Either one would have to perform molecular dynamics (MD) simulations or include heat conduction in the model, both making the treatment of large systems over long time scales infeasible. Instead, we choose a higher but constant effective temperature T, which is a good first approximation.

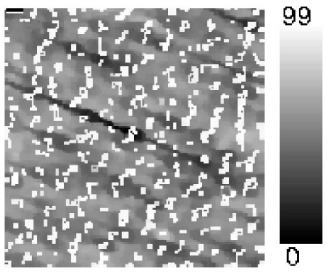

FIG. 3. Sample surface topology for a small system ($L=128$), for the Arrhenius MC diffusion mechanism at a surface temperature equal to room temperature, after $t=100$ ions/atom. No clear ripples can be observed. Similar results were observed for almost all times, except the very early ones.

Now, we want to estimate this effective temperature. The most basic approach is to describe the energy carried by the ions as a constant inflow of energy at the surface, fix the temperature far away from the surface to room temperature, and solve the stationary heat-conduction equation to calculate the temperature at the surface.[30] The resulting temperature depends strongly on the ion energy, the ion current density, and the thermal conductivity of the material. For experimentally reported parameters, temperature rises up to 1500 K ($0.155\ \mathrm{eV}\ k_B^{-1}$) are found.[30] This shows that high efficient temperatures, even in the stationary state, may be achieved. However, in the experiments of Habenicht *et al.*[23] only small average ion current densities were used, which resulted in a temperature rise at the surface of only a few K.

This does not mean that one can use a temperature close to room temperature as an effective temperature. The reason is that right after impact, the surface is strongly heated close to the melting temperature and then quickly cooled again, i.e., a *thermal spike* occurs.[31] Furthermore, the surface is sputtered using a focused ion beam (of diameter 30 nm), which is moved relatively slowly over the surface, and which exhibits a large spot current of 15 $\mu\mathrm{A}/\mathrm{cm}^2$. Hence, under the ion beam, for several short time intervals, surface diffusion is greatly enhanced. Marks calculated[32] the spatiotemporal development of the temperature after ion impact by solving the dynamic-heat-conduction equation, resulting in a temperature profile $\tilde{T}(r,t)$ as a function of time t and distance r from the point of impact. The initial distribution $\tilde{T}(r,0)$ is given by a step function with $\tilde{T}(r,0)$ being the melting temperature of the material for $r\leqslant r_0$ and being the room temperature elsewhere. The initial radius r_0 is determined such that the thermal energy inside this semisphere equals the energy carried by the ion. Marks found that the surface is heated strongly right after the impact and is cooled down to temperatures close to room temperature within few ps. Qualitatively and quantitatively similar profiles have been observed in MD simulations[33] as well. We apply Marks's equation, using the parameters for ion energy and ion current density in the spot as given above to determine an effective temperature (with $r_0=15.6$ Å in our case). The basic idea is that in a

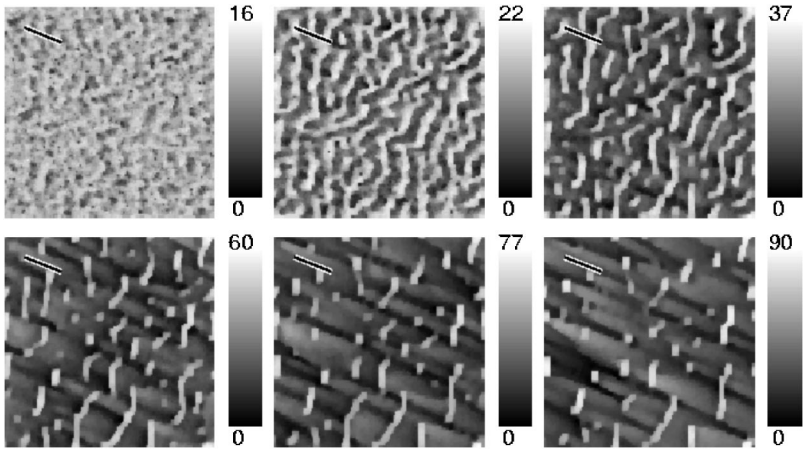

FIG. 4. Surface profiles at a substrate temperature of 0.1 eV/k_B with the second diffusion model. Starting from top to bottom and left to right, $t=0.5$, 1.5, 4.0, 9.0, 14.0, and 20.0 ions/atom. In both cases depicted here and in Fig. 1, ripples propagate along a direction opposite to that of the ion beam.

time interval Δt, the number of hops governed by the temperature $\tilde{T}(0,t)$ at the impact point should be the same as the number under the effective temperature T,

$$\int_0^{\Delta t} k_0 \exp\left(-\frac{\Delta E}{k_B \tilde{T}(0,t)}\right) dt = \Delta t k_0 \exp\left(-\frac{\Delta E}{k_B T}\right). \quad (8)$$

We have neglected here the temperature dependence of k_0. When including it, we find that the resulting effective temperature changes only slightly. We choose Δt as the average time between two ions arriving in a circle with area πr_0^2 under the ion-beam spot, resulting in $\Delta t = 1.4 \times 10^5$ ps. For the energy barrier, we choose $\Delta E = E_{SB} + 3E_{NN} + E_S$, which corresponds to atoms along the edges of the islands and/or steps. Using these parameters, we find an effective surface temperature of $T=1200$ K, i.e., which is considerably higher than room temperature. In this calculation it is assumed that only the energy carried by the ions hitting the "target area" πr_0^2 contribute to the heating of the surface inside the area. If one were to take into account that the ions hitting the neighborhood of the target area also contribute to the heating inside the area, then even higher effective temperatures can be expected.

The exact effective temperature depends on many parameters, such as ion energy, ion current density, heat conduction, surface roughness, etc. We are here interested only in universal effects, not in modeling a specific experimental setup. For this reason, we use the above result only as a guideline and study several temperatures of this order of magnitude and additional ones above it. Hence, for the further analysis of ripple movement, we consider high effective temperatures for the Arrhenius MC model, such that the surface diffusion is indeed able to act as an effective smoothing mechanism (see Fig. 4). At such higher temperatures we observe some universal features for both diffusion mechanisms, as presented now. Figure 5 is the plot of the ripple wavelength (circle symbols) versus time, measured in units of the number of ions per atom; its inset is a plot of the projection of the ripple velocity along the ion-beam direction versus time, both at the estimated effective temperature of $k_B T = 0.1$ eV, corresponding to the experimental conditions from Ref. 23.

A plot of wavelength versus time in Fig. 5 reveals that for short times $\lambda \sim t^{0.32}$, which is between the results $\lambda \sim t^{0.5}$ of Habenicht *et al.*[23] and $\lambda \sim t^{0.26}$ of Frost *et al.*[35] and Rusponi *et al.*[15] But we observe a power-law behavior only in the initial stages of ripple formation, the wavelength becoming constant in time at a later stage.

The velocity shows a power-law behavior over a larger time interval, resulting in $v \sim t^{-0.7}$, as obtained from the inset of Fig. 5. This is in excellent agreement with the experimental result $v \sim t^{-0.75}$ of Habenicht *et al.*[23]. A difference is that for smaller times a constant velocity was observed in the experiments, while we do not see any clean ripples for smaller times than the power-law regime. Anyway, combining both scaling results gives $v \sim \lambda^{-2.19}$, in good agreement with the exponent -2 of the continuum theory.[2]

Now we turn to higher effective substrate temperatures, corresponding, e.g., to higher ion currents and/or materials with lower heat-conductivity. Figures 6 and 7 are plots of the ripple wavelength (circle symbols) as a function of time, at respective temperatures $k_B T = 0.2$ J and $k_B T = 0.2$ eV, using the first and second models of the surface diffusion, respectively. In both models, the ripples disappear after a while, i.e., the ripple wavelength diverges. Considering the lifetime of the ripples from first appearance to annihilation, the wavelength increases exponentially with time as $\lambda \sim \exp(\rho t)$, $\rho = 0.029$ (Fig. 6), in the first model, while it increases with

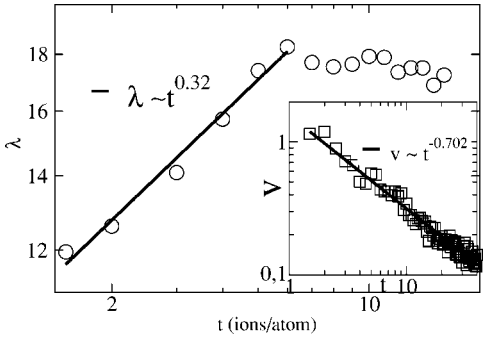

FIG. 5. Ripple wavelength λ measured in lattice units, as a fuction of time t. The inset shows the time dependence of the ripple-propagation velocity v (measured in lattice units per ion per atom). Both results are for the kinetic-diffusion mechanism, at a substrate temperature of $k_B T = 0.1$ eV.

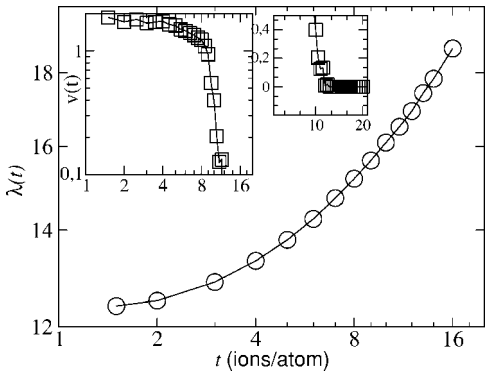

FIG. 6. Ripple wavelength λ measured in lattice units, as a fuction of time t. The inset shows the time dependence of the ripple-propagation velocity v (measured in lattice units per ion per atom). Both results are for the thermodynamic-diffusion mechanism at a substrate temperature of 0.2 J k_B^{-1}.

time according to the inverse law $\lambda(t) \sim 1/(c_1 - c_2 t)$ with $c_1 = 0.083$ and $c2 = 0.0036$ (Fig. 7) in the second model. To investigate the origin of the difference, we also perform simulations with the Arrhenius model, but with the Schwoebel term set to zero. In this case the result is very similar to the result in Fig. 6 of the thermodynamic model (which has no Schwoebel term here), and we obtain the behavior $\lambda \sim \exp(0.036t)$. On the other hand, when we set the energy in the Schwoebel term to twice its value, $E_{SB} = 0.3$ eV, the result is very similar to $E_{SB} = 0.15$ eV. This shows that the Schwoebel barrier plays an important role in the pattern formation process. Note that these fits are purely heuristic. We are not aware of any theory of the time dependence of ripple wavelength and velocity; only a calculation of the dispersion relation $v(\lambda)$ has been performed within linear theory.[2] Furthermore, there exists an analytic study of the temporal development of step bunches during epitaxial growth.[22,34]

The insets of Figs. 6 and 7 are plots of the ripple velocity (line with square symbols) as a function of time. Irrespective of which surface-diffusion mechanism is employed, the velocity is at first almost independent of time, and then it disperses after a transition time t_r. This initial plateau is similar to the plateau observed in the experiments, but the drop in velocity is very abrupt, and no clear power law is visible then. Moreover, the ripples finally come to rest before completely disappearing, as seen in the smaller inset of Fig. 6. We find, however, that at the lower temperature in the kinetic model, the ripples do not stop moving until their disappearance. Figure 8 shows the dependence of the ripple velocity on the wavelength for $k_B T = 0.2$ J; their order of magnitude relationship is about the same as in the experiment. We see in Fig. 9 that the trend in velocity variation is the same at high temperatures, but the magnitude increases with temperature, as one would expect from the temperature dependence of the surface diffusion. But we only observed a power-law scaling at temperatures below $k_B T \approx 0.18$ eV. This indicates that the presence of power-law scaling of ripple wavelength and ve-

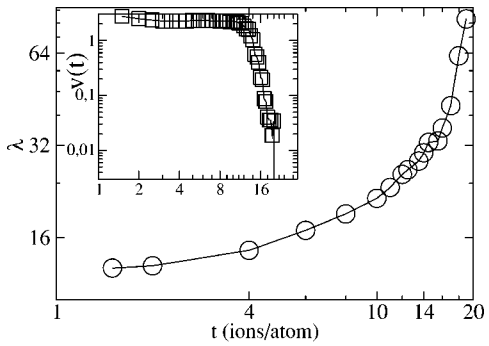

FIG. 7. Same plot as in Fig. 6, but for the Arrhenius diffusion mechanism for a substrate temperature of 0.2 eV/k_B. In both figures, the line with circle symbols represents the wavelength, while the line with square symbols represents the velocity.

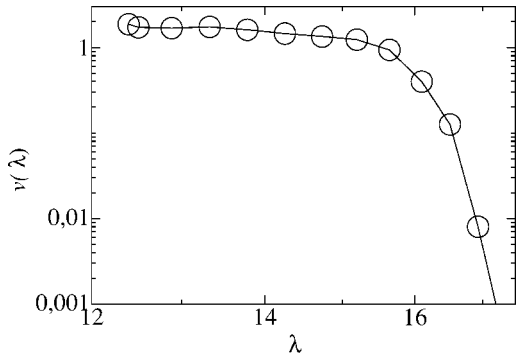

FIG. 8. Ripple velocity as a function of ripple wavelength, for the thermodyanmic-diffusion mechanism.

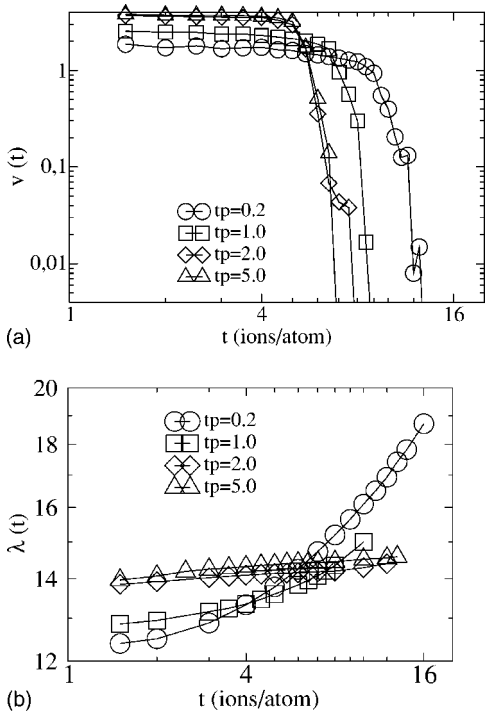

FIG. 9. Temperature dependence of the ripple velocity (upper graph) and ripple wavelength (lower graph) for the thermodynamic-diffusion mechanism. The temperature is in units of J k_B^{-1}.

locity, and the corresponding exponents, depends on the time scale of observation (Fig. 5), as well as on the effective temperature.

It seems that the increase in magnitude of the velocity, when measured at the same time ($t < t_r$) but a different temperatures, does not continue indefinitely in our model. In the upper graph of Fig. 9 there is very little difference in the magnitudes of the velocity at temperatures 2.0 and 5.0 J k_B^{-1}, even though the temperature difference is very high. This saturation behavior is also displayed in the ripple wavelength at higher temperatures, as seen in the lower graph of Fig. 9. In principle, one can still fit an exponential law to the data, except that the decay constant ρ in the exponential becomes very small. (It has the respective values of 0.029, 0.018, 0.0031, and 0.003 from the lowest to the highest temperatures.) So for very high effective temperatures we could equally well fit a power law. Hence, there may be some "critical substrate temperature," above which the wavelength remains nearly constant in time, and the velocity, after some time t_r, drops instantaneously to zero. Nevertheless, the temperature where such a "transition" would take place is probably unphysically high (see below), so that the material used in the experiment would start to evaporate before reaching this point. But other materials, in combination with high ion currents, might display such a behavior. So far, we are only aware of one set of experiments.[23] Hence, it would be very interesting to see whether some temperature dependence of the dynamical features, including the disappearance of the coarsening, can be seen in experiments at higher effective temperatures corresponding to high ion currents and/or higher lab temperatures.

Our results for the second diffusion model also indicate that in $\lambda(t) \approx 1/(c_1 - c_2 t)$, c_2 approaches zero with increasing temperature. Here, where we can measure the temperature in real units, it is clear that the "transition" to almost noncoarsening ripples takes place at unrealistically high temperatures such as $2-5$ eV$/k_B$, where the material starts to evaporate. Moreover, we notice in Fig. 9 that the transition time from linear the regime to the onset of nonlinearities decreases with increasing temperature.

To summarize, ripple propagation depends on the effective substrate temperature as well as the diffusion mechanism. Around temperatures realized experimentally thus far, ripples propagate, from their first appearance, with decreasing velocity until their disappearance without full cessation of motion. At high effective temperatures, however, immediately after ripple formation, the ripples move with constant velocity for some time, after which they begin to decelerate (insets of Figs. 6 and 7) and after some time, depending on the diffusion model, the ripples stop moving, but keep disappearing gradually. At the same time the ripple structure is gradually being washed out, and in the final stage the ripples are completely wiped out. The ripple wavelength is always increasing in time at high temperatures, while at low effective temperatures it initially increases with time and later becomes constant.

V. CONCLUSION AND OUTLOOK

We have studied the propagation of ripples by means of a discrete $(2+1)$-dimensional model of the sputtering process, combined with one of two different solid-on-solid models of surface diffusion: an Arrhenius MC mechanism with Ehrlich-Schwoebel barriers and a thermodynamic mechanism without a Schwoebel term. We obtained the formation and propagation of the ripples with both diffusion mechanisms used in turn. Furthermore, we obtained the same trend in the behavior of ripple velocity and wavelength, as observed experimentally and predicted theoretically, but, in addition to the experimental results, we found a drastic change in the ripple propagation at temperatures well above the so-far experimentally realized effective temperature; for instance we found deviations from power-law behavior into exponential or inverse-law behavior, and in addition, the ripples first stop moving before vanishing completely. We found that, at very high effective temperatures, the behavior of the ripple velocity is charaterized by two regions, separated at the transition time. In the first region it was constant, and in the second region it decreased rapidly to zero. Between the two regions a power-law dependence could be observed for a small time interval. Whereas, around the temperatures realized experimentally thus far, the velocity-time relationship obeyed a power law. Furthermore, at high effective temperatures, the wavelength increased exponentially with time in the thermodynamic-diffusion model (and in the Arrhenius diffusion model without a Schwoebel term), and it obeyed an inverse law for the Arrhenius model including the Schwoebel barrier. In addition, we found further strong dependencies on the effective substrate temperature; as the temperature increased the magnitude of the velocity also increased. The transition time between constant and decreasing velocity was also found to decrease with increasing temperature. Our results indicate an approach towards a saturation behavior of the velocity or wavelength with an increasing effective substrate temperature, where the wavelength is expected to become time independent. However, this may happen at an unphysically high temperature. Anyway, an experimental study of the dependence of the dynamical features of ripple formation and effacement on the physical conditions seems very promising.

One open problem of our model at high incidence angles (e.g, $\theta > 75°$), is that it uses the Sigmund formula for modeling the sputtering process. In a recent simulation[36] using a binary-collision approximation, we observed that close to the penetration point of the ion, many fewer atoms were sputtered than predicted by the Sigmund formula (1); in fact the distribution showed a minimum there. When incorporating this effect in the Bradley-Harper linear theory[20] of sputtering, e.g., one observes[36] that the sputter yield, i.e., the number of removed atoms per ion, exhibits a minimum for grazing incidence, as in the experiments, in contrast to the orginial linear theory.[20] Hence, it may be promising to apply a different formula describing the sputtering, which takes this effect into account.

Furthermore, the role of the interplay between the surface-diffusion process and the sputtering process is still not fully understood. So far, we know that including a pure $T=0$ relaxation in our sputtering model does not[24] lead to a disappearance of ripples for long times. Next, we know from this study, that one approach including the calibrated

Schwoebel barriers does not yield ripples at room temperature for the sputtering yield $Y \approx 7$. There are several different models[27,28,37–42] for surface diffusion that could be combined in a construction-kit manner. Here, an extensive study over different combinations of parameters is necessary.

Finally, it would be of interest to include crystal anisotropy into the surface diffusion. This may give results, in agreement with experimental studies of metallic substrates, which may be useful in understanding the anomalies of such surfaces.

ACKNOWLEDGMENTS

The authors would like to thank K. Lieb and R. Cuerno for helpful discussions and suggestions. E.O.Y. thanks Henning Löwe for interesting discussions. The large-scale numerical simulations were performed on the workstation clusters of the institute. This work was funded by the DFG (Deutsche Forschungsgemeinschaft) within the SFB (Sonderforschungbereich) 602 and by the VolkswagenStiftung (Germany) within the program "Nachwuchsgruppen an Universitäten."

*Electronic address: yewande@theorie.physik.uni-goettingen.de

[1] A.-L. Barabási and H. E. Stanley, *Fractal Concepts in Surface Growth* (Cambridge University Press, Cambridge, 1995).
[2] M. Makeev, R. Cuerno, and A.-L. Barabási, Nucl. Instrum. Methods Phys. Res. B **197**, 185 (2002).
[3] S. Facsko, T. Dekorsy, C. Koerdt, C. Trappe, H. Kurz, A. Vogt, and H. L. Hartnagel, Science **285**, 1551 (1999).
[4] T. M. Mayer, E. Chason, and A. J. Howard, J. Appl. Phys. **76**, 1633 (1994).
[5] E. Chason, T. M. Mayer, B. K. Kellerman, D. T. McIlroy, and A. J. Howard, Phys. Rev. Lett. **72**, 3040 (1994).
[6] C. M. Demanet, J. B. Malherbe, N. G. Vanderberg, and V. Sankar, Surf. Interface Anal. **23**, 433 (1995).
[7] S. W. MacLaren, J. E. Baker, N. L. Finnegan, and C. M. Loxton, J. Vac. Sci. Technol. A **10**, 468 (1992).
[8] J. B. Malherbe, CRC Crit. Rev. Solid State Mater. Sci. **19**, 55 (1994), and references therein.
[9] G. Carter and V. Vishnyakov, Phys. Rev. B **54**, 17 647 (1996).
[10] J. Erlebacher, M. J. Aziz, E. Chason, M. B. Sinclair, and J. A. Floro, Phys. Rev. Lett. **82**, 2330 (1999), and references therein.
[11] S. Habenicht, W. Bolse, K. P. Lieb, K. Reimann, and U. Geyer, Phys. Rev. B **60**, R2200 (1999).
[12] According to the linear theory of Bradley and Harper, θ_c occurs at the point of intersection of the two functions $\Gamma_1(\theta)=(\alpha/\gamma)\{s-(c/2)[1+\eta]-[sc(\beta-\alpha)/2\gamma][3+\eta]\}$ and $\Gamma_2(\theta)=(\alpha c/2\beta)\{1+[s(\beta-\alpha)/\gamma]\}$; where $s=\sin^2(\theta)$, $c=\cos^2(\theta)$, $\alpha=(d/\sigma)^2$, $\beta=(d/\mu)^2$, and $\gamma=\alpha s+\beta c$, $\eta=(\alpha^2 s/\gamma)$. d, σ, and μ are as described in this paper. Depending on the choice of σ and μ, there may be two critical angles.[20]
[13] S. Rusponi, C. Boragno, and U. Valbusa, Phys. Rev. Lett. **78**, 2795 (1997).
[14] S. Rusponi, G. Costantini, C. Boragno, and U. Valbusa, Phys. Rev. Lett. **81**, 2735 (1998).
[15] S. Rusponi, G. Costantini, C. Boragno, and U. Valbusa, Phys. Rev. Lett. **81**, 4184 (1998).
[16] E. A. Eklund, R. Bruinsma, J. Rudnick, and R. S. Williams, Phys. Rev. Lett. **67**, 1759 (1991).
[17] E. A. Eklund, E. J. Snyder, and R. S. Williams, Surf. Sci. **285**, 157 (1993).
[18] J. Krim, I. Heyvaert, C. Van Haesendoncek, and Y. Bruynseraede, Phys. Rev. Lett. **70**, 57 (1993).
[19] H.-N. Yang, G.-C. Wang, and T.-M. Lu, Phys. Rev. B **50**, 7635 (1994).
[20] R. M. Bradley and J. M. E. Harper, J. Vac. Sci. Technol. A **6**, 2390 (1988).
[21] R. Cuerno and A.-L. Barabási, Phys. Rev. Lett. **74**, 4746 (1995).
[22] A. Pimpinelli, V. Tonchev, A. Videcoq, and M. Vladimirova, Phys. Rev. Lett. **88**, 206103 (2002).
[23] S. Habenicht, K. P. Lieb, J. Koch, and A. D. Wieck, Phys. Rev. B **65**, 115327 (2002).
[24] A. K. Hartmann, R. Kree, U. Geyer, and M. Kölbel, Phys. Rev. B **65**, 193403 (2002).
[25] P. Sigmund, Phys. Rev. **184**, 383 (1969).
[26] J. F. Ziegeler, J. P. Biersack, and K. Littmark, *The Stopping and Range of Ions in Matter* (Pergamon, New York, 1985); see also http://www.srim.org/
[27] M. Siegert and M. Plischke, Phys. Rev. E **50**, 917 (1994).
[28] P. Šmilauer, M. R. Wilby, and D. D. Vvedensky, Phys. Rev. B **47**, 4119 (1993).
[29] T. Shitara, D. D. Vvedensky, M. R. Wilby, J. Zhang, J. H. Neave, and B. A. Joyce, Phys. Rev. B **46**, 6815 (1992).
[30] J. Melngailis, J. Vac. Sci. Technol. B **5**, 469 (1987).
[31] W. Primak, Phys. Rev. **98**, 1854 (1955).
[32] N. A. Marks, Phys. Rev. B **56**, 2441 (1997).
[33] D. Saada, J. Adler, and R. Kalish, Phys. Rev. B **59**, 6650 (1999).
[34] The growth equation studied in Ref. 22 is very different from the equations describing sputtering (self-similar behavior instead of periodic structures was studied), and the average terrace width decreases with time, while the wavelength increases in our case.
[35] F. Frost, A. Schindler, and F. Bigl, Phys. Rev. Lett. **85**, 4116 (2000).
[36] M. Feix, A. Hartmann, R. Kree, J. Muñoz-García, and R. Cuerno, Phys. Rev. B **71**, 125407 (2005).
[37] S. Das Sarma and P. Tamborenea, Phys. Rev. Lett. **66**, 325 (1991).
[38] M. R. Wilby, D. D. Vvedensky, and A. Zangwill, Phys. Rev. B **46**, 12 896 (1992); **47**, 16 068(E) (1993).
[39] M. V. Ramana Murty and B. H. Cooper, Phys. Rev. Lett. **83**, 352 (1999).
[40] K. Malarz and A. Z. Maksymowicz, Int. J. Mod. Phys. C **10**, 659 (1999).
[41] S. V. Ghaisas, Phys. Rev. E **63**, 062601 (2001).
[42] P. Punyindu, Z. Toroczkai, and S. Das Sarma, Phys. Rev. B **64**, 205407 (2001).